IEEE TRANSACTIONS ON
NUCLEAR SCIENCE

Novel Neutron Detector Material: Microcolumnar $Li_xNa_{1-x}I$:Eu

Matthew S. J. Marshall[1], Mitali J. More[1], Harish B. Bhandari[1], Richard A. Riedel[2], Shane Waterman[1], John Crespi[1], Peter Nickerson[1], Stuart Miller[1], and Vivek V. Nagarkar[1]

***Abstract*— Current neutron detection relies on ^{3}He detectors, which are prone to material shortages, and suffer from poor spatial resolution. Such inadequacies make ^{3}He unsuitable for new applications in state-of-the-art spallation sources such as the Spallation Neutron Source (SNS) at Oak Ridge National Laboratory (ORNL). Here, we report on the synthesis and application of a novel scintillator material for neutron detection: a mixed halide compound, Eu-doped (0.05 mol. %) $^6Li_xNa_{1-x}$ (^{6}LNI:Eu). ^{6}LNI:Eu is a bright, efficient, scintillator that can be grown in large format, thin films that exhibit microcolumnar structure in their cross-section. The ability to grow in a microcolumnar structure means that a resolution of approximately 5 lp/mm can be achieved with neutrons using an electron-multiplying charge coupled device (EMCCD) camera camera, thereby conferring an advantage over other solid (not gaseous) neutron scintillators, such as $Cs_2{}^6LiYCl_6$:Ce (CYLC) and GS20. The large area format of ^{6}LNI:Eu is a significant advantage for detecting specular reflections in neutron scattering experiments. Moreover, the microcolumnar nature of films permits high resolution imaging when films are coupled to a-Si:H flat panels, CCD, or CMOS readouts. While not the primary application, this also makes them suitable for digital neutron radiography. Enriched ^{6}Li was used to increase the neutron absorption cross section of the thin films, while preserving the brightness of the scintillation response. Here, we describe the vapor deposition techniques used to fabricate the ^{6}LNI:Eu scintillator screens and report on the test results. The films were tested at the High Flux Isotope Reactor (HFIR) at ORNL. An efficiency of approximately 43% for 4.1 Å neutrons with a resolution of 650 μm was measured for a 375 μm thick film of ^{6}LNI:Eu using a neutron sensitive Anger camera.**

I. Introduction

New high-intensity neutron sources, such as the SNS at ORNL, as well as other international spallation sources require new detector materials because of ^{3}He shortages, which is used in most current neutron scattering detectors. Moreover, ^{3}He can suffer from low spatial resolution. At the heart of an ideal neutron detector is a novel scintillator that exhibits high light yield, and has the ability to discriminate between neutron and gamma interactions based on pulse height, and shape. Moreover, such a detector must be made into a large format in a cost effective manner. Here, we address these challenges through the use of microcolumnar Eu-doped (0.05 mol. %) ^{6}LNI:Eu thin films for neutron detection [1]. For comparative purposes, all thin films discussed in this manuscript have a measured composition of $^6Li_{0.47}Na_{0.53}I$:Eu (0.05 mol. %) and are referred to throughout the manuscript simply as ^{6}LNI:Eu. The purity of lithium was 95% ^{6}Li.

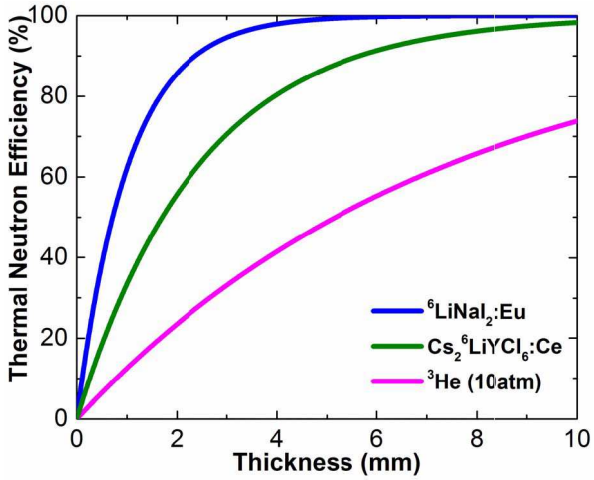

Fig. 1. Calculated plot showing the theoretical neutron absorption efficiency for ^{6}LNI:EU, CYLC, and ^{3}He at 10 atm.

^{6}LNI:Eu was chosen because ^{6}Li can be used to increase the absorption of neutrons within the framework of a chemically compatible bright scintillator (NaI). For instance, europium-doped lithium iodide (LiI) has a brightness of 15,000 photons/MeV, compared with 44,000 photons/MeV for europium doped sodium iodide [2]. Moreover, ^{6}LNI compares favorably to other lithium containing scintillators, where the $Cs_2{}^6LiYCl_6$:Ce (CLYC) lattice contains 1 ^{6}Li atom per 10 constituents, ^{6}LNI:Eu contains at least 1 out of 4 constituent atoms. Thus, the absorption of ^{6}LNI:Eu theoretically exceeds that of CYLC. The microscopic thermal neutron absorption cross-section ^{6}Li is 940 barns, while that of ^{3}He is 5333 barns [3]. While there is a factor of five difference in the *microscopic* thermal neutron absorption cross sections, the *macroscopic* thermal neutron absorption cross sections are closer in magnitude due to the increased atomic density of ^{6}Li in ^{6}LNI:Eu in comparison to gaseous ^{3}He. The difference in macroscopic absorption cross-sections is clearly shown by the plot in Figure 1. In Fig. 1, the theoretical neutron absorption efficiency has been calculated for ^{6}LNI:Eu with $\sim$ 50:50 of ^{6}Li:Na, CLYC, and ^{3}He gas at 10 atm pressure, all calculated for thermal neutrons (0.0254eV), at which the absorption cross-section for lithium is 940 barns. From Fig. 1,

This work was supported by Department of Energy under grants DE-SC0011311 and DE-SC0008291.

Vivek V. Nagarkar (phone: 617-668-6937; VNagarkar@rmdinc.com) and all the remaining authors are with Radiation Monitoring Devices, Inc. (RMD), Watertown, MA 02472, USA.

Richard A. Riedel, Neutron Scattering Science Division, Oak Ridge National Laboratory, PO Box 2008, Building 7962, Oak Ridge, TN 37831-6393, USA.

Digital Object Identifier: 10.1109/TNS.2017.2762859

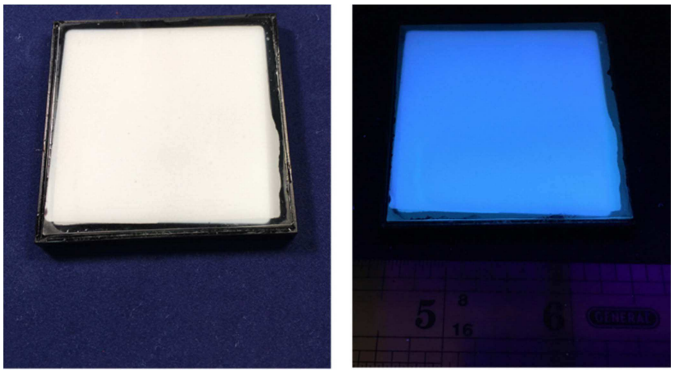

Fig. 2. Picture of a ^{6}LNI:Eu scintillator screen deposited on a fiber optic faceplate. The film is 2 inch square and is packaged in an anodized aluminum holder, sealed in a nitrogen atmosphere with an airtight epoxy. A photo of the film under visible illumination is shown in (a), with the corresponding picture taken under UV illumination (365 nm wavelength) in (b), which shows emission at 450 nm.

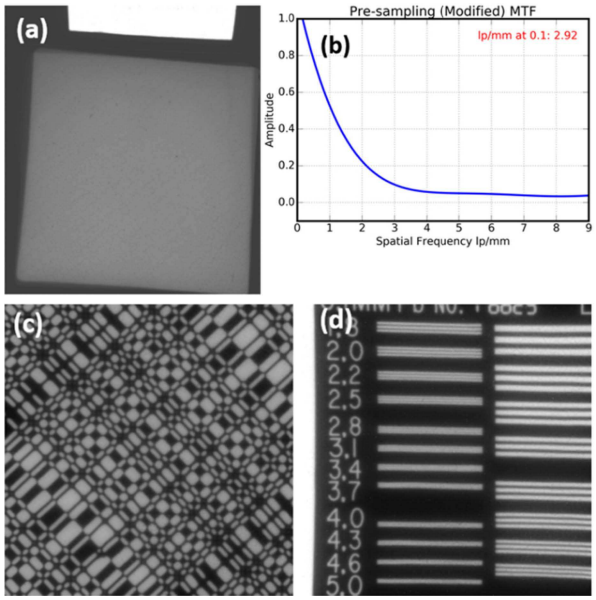

Fig. 3. (a), (c) (d) X-ray images taken at 70 kVp, and 10 mA, all using the same 375 um thick $Li_{0.45}Na_{0.45}I:Eu_{0.05}$ scintillator screen prepared on a fiber optic faceplate. (a) X-ray flood of the ^{6}LNI:Eu screen compared to a MinR-2000 reference for calibration of the brightness. MTF plot of this same film is shown (b), with a resolution of 2.92 lp/mm at 10% MTF, and two phantoms in (c) and (d) used to gauge the uniformity and the resolution.

the theoretical calculations of the neutron absorption efficiency indicate that a 1 mm thick film of ^{6}LNI will exhibit twice the neutron absorption efficiency of a 1 mm thick piece of CYLC. The ability to grow in a thin film microcolumnar format also provides some practical advantages in terms of the resolution of the film.

The two most well-known neutron-gamma discrimination methods are based on pulse-shape discrimination (PSD) and pulse-height discrimination (PHD). In this manuscript, we show the efficacy of PHD by measuring the gamma equivalent energy (GEE) of the film. A neutron event has a reaction Q-value of ∼4.7 MeV in ^{6}Li, whereas lower energy gammas, relative to the reaction Q-value, have a lower light yield and therefore lower signal from the photomultiplier tube (PMT) upon irradiation. The alpha and triton decay products have a combined energy of 4.5 MeV, which is deposited locally in the material. Thus, in total, 4.5 MeV of energy is imparted to the ionized electrons, which then go through recombination processes that yield scintillation light. Since the neutron interaction has substantially more ionizations involved with its interaction in ^{6}LNI than a lower energy gamma-ray, it has a much larger output signal. Thus, the obvious difference in pulse heights makes PHD a viable option.

While, the neutron cross section for ^{6}Li is lower than, for instance, ^{157}Gd, ^{6}Li has numerous advantages over ^{157}Gd for neutron detection. The ^{6}Li reaction has an alpha particle as a by-product while the by-products of neutron interactions with ^{157}Gd-containing compounds include low-energy electrons and gamma rays. The primary advantage of using ^{6}Li over ^{157}Gd is that the alpha decay from ^{6}Li produces a pulse that is significantly brighter and has a different shape than a gamma interaction. This is because of the higher linear energy transfer. This makes it possible to determine whether a particle is a neutron or gamma based on *either* pulse height or pulse shape discrimination. Because Gd is unable to discriminate between neutron and gamma events, it also does not work in applications with a high gamma background.

II. Material Synthesis and Characterization

Thin films of microcolumnar ^{6}LNI:Eu were synthesized using thermal evaporation. In particular, two methods were used to grow the thin films, co-evaporation of large area films (unpublished) and hot wall evaporation (HWE). The focus of this manuscript is on films grown using HWE. In a typical HWE setup (described in [4, 5]), the high purity raw materials are loaded into a quartz crucible with the substrate placed directly on top of the crucible. Covering the crucible opening with the substrate prohibits wastage of evaporated materials. Material deposited on the walls of the crucible re-evaporates, thereby conserving material. Here, we focus on a modified, or pseudo, hot wall evaporation set-up, in which the sample does not sit directly atop the crucible, but rather, is several inches above the top. This pseudo-HWE allows us to shutter the crucible, enabling a more compositionally uniform deposition. The pseudo-HWE setup also prevents overheating of temperature sensitive fiber optic substrates by creating distance above the crucible. While this reduces the deposition efficiency, it facilitates growth of thick films without significant loss of material. The thin films were deposited onto fiber optic faceplate, sapphire, and fused silica, and were subsequently packaged into a hermetically sealed anodized aluminum box to protect the films, which are extremely hygroscopic, from moisture. Using this approach, we have produced 1.5” diameter and 2” square films of packaged ^{6}LNI:Eu. In Fig. 2, images are shown of a ^{6}LNI:Eu film grown on fiber optic faceplate packaged in an anodized aluminum holder

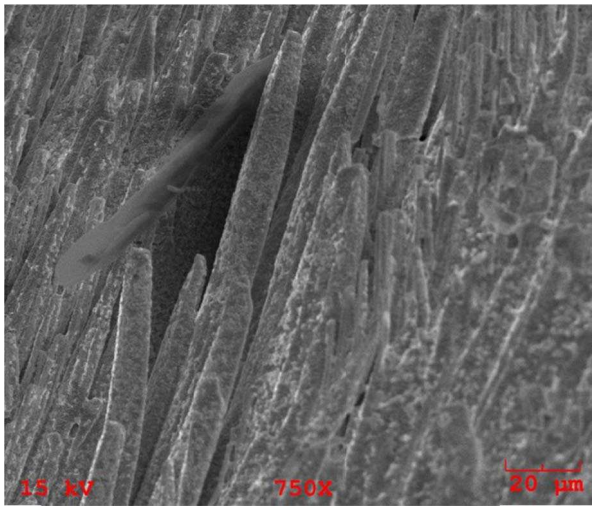

Fig. 4. Scanning Electron Micrograph of a 1.5 mm thick ^{6}LNI:Eu film showing columnar structure, with a column diameter on the order of 10 – 20 μm.

III. Scintillator Characterization

A. X-ray Imaging

To demonstrate the imaging capabilities of the ^{6}LNI:Eu films a series of X-ray images were taken using a 375 um thick film. X-ray imaging is widespread, and offers a rapid method of assessing the uniformity and physical characteristics of the film. In particular, the resolution of these scintillator screens depends on the columnar structure of the film, and X-ray imaging is a quick way to assess this. The film, which was deposited directly on a fiber optic faceplate and packaged, was coupled with refractive index matching fluid to a Photometrics CCD via a 3:1 fiber optic taper. A Gendex dental X-ray generator was used at a source-to-detector distance of 45 cm with 70 kVp (10 mA).

Fig. 3(a) shows a flood image of the film, compared to MinR-2000 commercial Gd_2O_2S:Tb screen. MinR-2000 is used as a calibration of the brightness of individual films. The scintillator screen in Fig. 3(a) achieved 30% of the brightness of MinR-2000 without correcting for the low-sensitivity of the CCD detector to blue light emitted by the ^{6}LNI:Eu. Measurements from a 2.75 mm thick ^{6}LNI:Eu film using a ^{57}Co source revealed the light output to be 19,400 photons/MeV. To demonstrate the X-ray imaging capabilities of these scintillator screens, a series of phantom images were taken, as shown in Figs. 3(b) – (d). X-ray images were flat-field corrected to remove any fixed pattern structures in the raw image and thereby enhance contrast. An X-ray image of a key is shown in Fig. 3(b), a patterned X-ray coded aperture mask is shown in Fig. 3(c), and a line-pair phantom is shown in Fig. 3(d). The emission of the film was also measured to be 450 nm.

B. Resolution measurement with X-rays

The spatial resolution of the ^{6}LNI:Eu films was quantified in terms of the pre-sampling modulation transfer function (MTF). MTF measurements were done according to the technique described by Fujita *et al* [6]. A detailed description of the specific experimental procedure has been previously described [7, 8, 9]. To obtain the MTF, an image of a 10 μm ($\pm$1 μm) wide slit made of 1.5 mm thick tantalum placed at a slight angle (less than 4°) to the pixel matrix at the center of the detector was obtained. The area around the slit was covered with 0.5 cm thick lead. The slit was placed in contact with the surface of the imager so that the spreading of the Line Spread Function (LSF) due to the finite size of the focal spot did not pose a significant limitation. The MTF showed 10% modulation at $\sim$3 lp/mm.

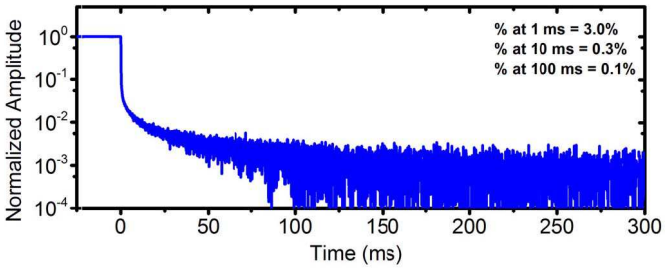

Fig. 5. Afterglow measurement on a 1.5"Ø ^{6}LNI:Eu film (256 μm thick) shows that the residual signal is $\sim$0.1% of the maximum intensity at 100 ms post-irradiation.

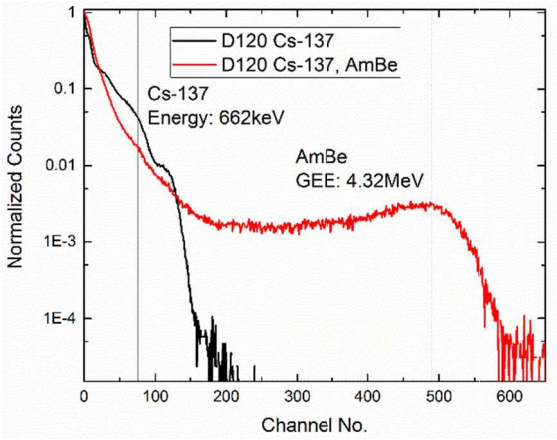

Fig. 6. The normalized response to neutrons of the 375 μm thick LNI:Eu film shown in Fig. 2 . There is a clear difference between the neutron response peak, at approx. 4.3 MeV gamma equivalent energy and the response peak to the gamma irradiation with Cs-137.

C. Morphology Measurement

Following deposition of a 1.5 mm thick ^{6}LNI:Eu film, scanning electron microscopy (SEM) was performed on a portion of a sacrificial film, and is shown in Fig. 4. The columnar structure of the film is readily apparent in Fig. 4, with a column diameter of approx. 10 – 20 μm. The columnar nature of the scintillator screen has the effect of channeling scintillation light via total internal reflection vertically towards the fiber optic, with the effect of dramatically enhanced spatial resolution as is demonstrated in the measured resolution of the film.

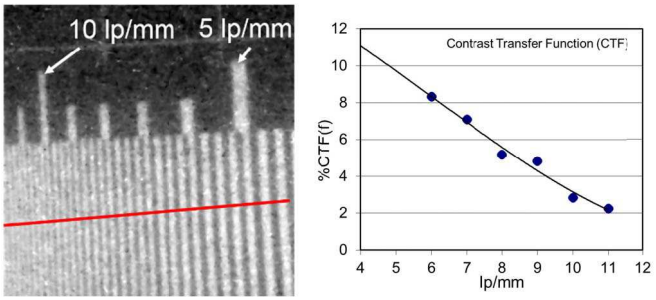

Fig. 7. (a) Image of a Gd resolution mask obtained with a LNI:Eu film coupled to a EMCCD camera. **(b)** The % modulation calculated as a function of the resolution. With this film, we can resolve up to 5 lp/mm at 10% CTF

D. Afterglow Measurement

Afterglow is quoted in terms of residual signal at a specified time after excitation cut-off, relative to that during excitation. Measurements were done with a photodiode and preamp setup connected to a data acquisition card (National Instruments model PCI-5122). Each sample was excited using an Electromed X-ray generator with pulse parameters set at 100 kVp, 200 mA, and 100 ms. All afterglow values for the samples were reported as the residual signal at an elapsed time of 1 ms immediately after excitation cut-off. Figure 5 shows an afterglow plot from a 1.5"Ø^{6}LNI:Eu film (256 μm thick). The measured afterglow for this sample was $\sim$ 0.1% at 100 ms after irradiation.

E. Neutron Response

The neutron response of the ^{6}LNI:Eu film is shown in Fig. 6. This was obtained using a 4.7 μCi ^{137}Cs source for gamma irradiation and a 96 mCi ^{241}AmBe source for neutron irradiation. The data was processed using AMPTEK's DppMCA data analysis software. The resulting photopeak positions for the 662 keV Cs source and that for the thermal neutrons were compared to estimate the gamma equivalent energy (GEE). A clear separation is visible for the neutron peak at 4.3 MeV and the gamma peak (662 keV), showing that these films discriminate between 662 KeV gammas and neutrons based on pulse height. Such neutron-gamma discrimination is a key requirement for scattering detector applications. Although the *films* have shown GEE of 4.3 MeV (Fig. 6), we have measured emissions of 102,400 photons per thermal neutron giving a GEE of 4.5 MeV on other LNI *single crystals*, very close to the 4.7 MeV Q-value of the Li-neutron interaction [1]. Furthermore, measurements at ORNL determined that the efficiency of 4.1 Å neutron detection was $\sim$43% for a 375 um-thick film of ^{6}LNI:Eu [10].

F. Neutron Imaging

The neutron imaging properties of the ^{6}LNI:Eu scintillator were evaluated using a fiberoptic coupled EMCCD camera consisting of an Andor back-illuminated, thermoelectrically cooled, 1024$\times$1024 pixel EMCCD with 13 μm pixels as a readout sensor coupled to the scintillator via a detachable 3:1 fiberoptic taper. With the taper in place, the detector has an effective pixel size of 39 μm. The EMCCD detector was setup at HFIR's CG1a beamline which supplied 4.1 Å neutron flux at 10^{5} n/cm^{2}/s. Figure 7(a) shows an image of a Gd resolution mask obtained with this setup. The percent modulation calculated as a function of the resolution is shown is Fig. 7(b). With this film, we can resolve up to 5 lp/mm at 10% CTF.

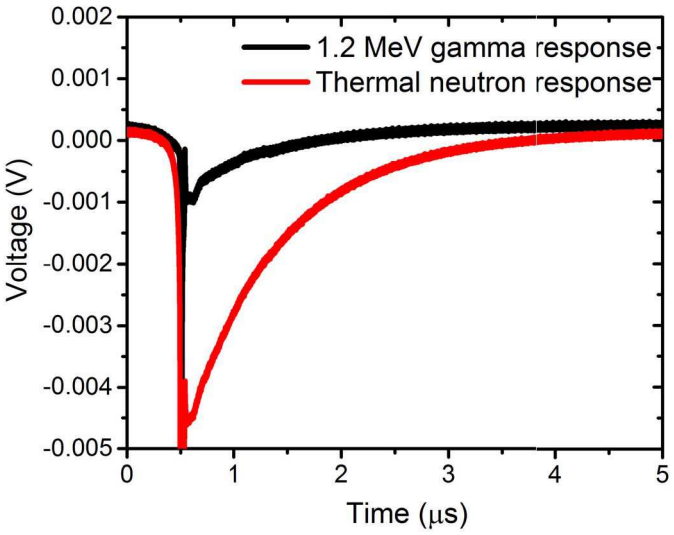

Fig. 8. Shows the difference in pulse shapes between the neutron and gamma events obtained with a 640 μm thick ^{6}LNI:Eu scintillator. This pulse shape can be effectively used to reject the gamma events and improve signal-noise ratio.

G. Pulse Shape Difference

An important aspect of the ^{6}LNI:Eu films is their use in pulse shape discrimination (PSD), which is useful when using an Anger camera for neutron diffraction or scattering measurements. Currently, GS20 neutron sensitive scintillators are only capable of pulse height discrimination, and can achieve gamma discrimination up to 10^{-3}. With the ability to additionally discriminate against gammas using PSD, the gamma rejection capability can be improved by two orders of magnitude. In Fig. 9, the signal from a 640 μm thick ^{6}LNI:Eu scintillator shows the response under excitation from a ^{60}Co source (gammas) and a Cf-252 source (neutrons), in which the shape of the pulses is dramatically different. This pulse shape difference can then be exploited to discriminate against gamma events when using na Anger camera.

IV. Conclusions

In conclusion, we have demonstrated the use of ^{6}LNI:Eu as a high resolution, bright neutron imaging scintillator, with a neutron resolution of 5 lp/mm, at a neutron absorption efficiency of $\sim$43% for 4.1 Å neutrons using an only 375 μm thick film. This is in conjunction with X-ray radiographic imaging that demonstrated the capabilities of these scintillator screens. The high resolution of the screens may be partially explained by the results obtained using scanning electron microscopy, which showed evidence of the microcolumnar structure that channels the scintillation light. The substantial

differences in the neutron and gamma interactions makes ^{6}LNI:Eu an ideal material for n-γ discrimination. While we have focused on scintillator screens formed using pseudo-HWE in this manuscript, co-evaporation can be used to achieve very large scintillator screen sizes useful for neutron radiography and neutron detection (scattering and diffraction).

REFERENCES

[1] V. Nagarkar, V., Ovechkina, E., Bhandari, H., Miller, S., Marton, Zs., Glodo, J., Soundara-Pandian, L., Mengesha, W., Gerling, M., Brubaker, E., 2013. Lithium alkali halides – new thermal neutron detectors with n-γ discrimination, Nuclear Science Symposium and Medical Imaging Conference (NSS/MIC), 2013 IEEE.

[2] Scintillation Properties. http://scintillator/lbl.gov

[3] Neutron scattering lengths and cross sections. *Neutron News,* Vol. 3, No. 3, pp. 29-37

[4] Bhandari, Harish B., et al. "Hot Wall Evaporation of High-Sensitivity, High-Resolution CeBr Scintillator." IEEE Transactions on Nuclear Science 59.5 (2012): 2196-2200.

[5] Nagarkar, V. V., et al. "Microcolumnar and polycrystalline growth of LaBr 3: Ce scintillator." Nuclear Instruments and Methods in Physics Research Section A: Accelerators, Spectrometers, Detectors and Associated Equipment 633 (2011): S286-S288.

[6] Fujita H., Tsai D.Y, Itoh T., Doi K., Morishita J., Ueda K., and Ohtsuka A., "A simple method for determining the modulation transfer function in digital radiography," IEEE Trans. Med. Imaging, 11, 34-39, 1992.

[7] Vedantham S., Karellas A., Suryanarayanan S., Albagli D., Han S., Tkaczyk E., Landberg C., Opsahl-Ong B., Granfors P., Levis I., D'Orsi C.J., and Hendrick R.E., "Full Breast Digital Mammographic Imaging with an Amorphous Silicon-based Flat Panel Detector: Physical Characteristics of a Clinical Prototype," Med. Phys. 27, 558-567, 2000.

[8] Vedantham S., Karellas A., Suryanarayanan S., Sayag M., Kleehammer R., Heidsieck R., and D'Orsi C.J., "Mammographic imaging with a small format CCD-based digital cassette: Physical characteristics of a clinical system," Med. Phys. 27(8), 1832-1840, 2000.

[9] Dobbins J.T., Ergun D.L., Rutz L., Hinshaw D.A., Blume H., and Clark D.C., "DQE(f) of four generations of computed tomography acquisition devices," Med. Phys. 22(10), 1581-1593, 1995.

[10] R. Riedel *et al.*, A first look at the neutron sensitive scintillator LiNaI in an Anger Camera detector. IEEE NSS, N28-20 (2016)